Statistical Treament of Cosmic Ray Scattering*

Charlie Sowerby†
UCLA Department of Physics
(Dated: March 17, 2021)

When high energy cosmic rays enter the upper atmosphere, this interaction produces π mesons, which eventually decay into muons that travel to the surface. In this experiment, we use scintillators attached to PhotoMultiplier Tubes (PMTs) to observe the muons passing through the laboratory. To calibrate the devices, we use the ratio of three-fold to two-fold coincidence to determine proper high-voltage trigger for the PMTs. This apparatus was then used to count the number of muons passing through during two different time intervals. A normalized histogram of the number of counts in each time interval is generated and compared to Gaussian and Poisson distributions respectively. In this experiment we study features of the Gaussian and Poisson distributions.

I. INTRODUCTION

To perform this experiment, we used plastic scintillators, which are devices that exploit the band structure of materials to convert high energy radiation into low-energy (near visible) light. These devices produce an analog signal proportional to the energy deposited by the incoming muon. This signal is fed into a PMT that uses a photocathode to convert the low energy photon into an electron. That electron bounces between several dynodes by means of an electric field, increasing the number of electrons each time, until the signal is collected at an anode. A discriminator is then used to convert the voltage in the anode to a digital signal. That digital signal is recorded and counted as a muon detection.

In this experiment, we stacked three of these setups on top of each other, so the incident muons would ideally pass through multiple scintillators and get recorded by multiple discriminators at what is effectively the exact same time. We define a two-fold coincidence when the both scintillators 1 and 2 fire at the same time, meaning a muon has passed through both. We define a three-fold coincidence when all three scintillators fire at the same time.

We need to calibrate the discriminator on scintillator 3 with the correct cutoff voltage as to eliminate noise while also ensuring that scintillator 3 fires as often as possible when a muon passes through scintillators 1 and 2. After calibration, we define a count anytime we see a two-fold coincidence.

We have chosen two time intervals and $\Delta t_1 = 0.72$s and $\Delta t_2 = 31.3$ s and counted the number of muons observed during each time interval, Δt_i. After repeating this several times, we plotted histograms of number of counts for each ΔT_i and fitted them to Poisson and Gaussian distributions respectively.

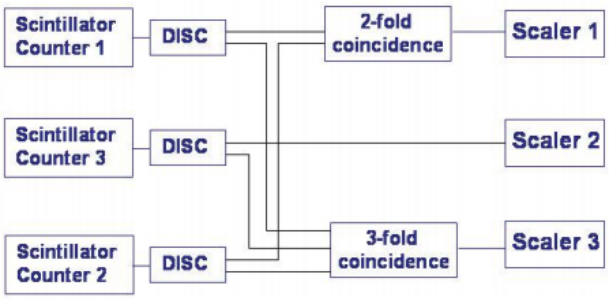

FIG. 1. Example diagram of two-fold and three-fold coincidences. A two-fold coincidence can occur between any two of the detectors.

II. EXPERIMENTAL SETUP

As a muon passes through a scintillator connected to a PMT, the result is an analog voltage that is fed into a discriminator that converts the voltage to a digital signal. In order to count as many muons as possible, while eliminating noise, the discriminator needs to be calibrated with a cutoff voltage such that noise is unable to produce enough voltage to trigger, but a muon count will register.

Since we are only interested in the distribution of counts, we only need to record a number of counts that is proportional to the total number of muons passing through the room. In other words, if a muon triggers the scintillators on the top and the bottom, we want the scintillator in the middle also to fire. If a muon passes through but doesn't have enough energy to trigger a two-fold coincidence, we can ignore it. If we calibrate the middle scintillator to fire only when when the ones above and below fire, then the high voltage cutoff for the middle scintillator will determine any count, as if the muon has enough energy to set off a two-fold coincidence after calibration, it either has enough energy to set off the top and bottom scintillators, hence it should also set off the middle one, or it sets of the middle one and one of the others, but if the muon sets off the middle scintillator, then it should have enough energy to set off the top and

* Physics 180a Experiment 1
† charlie.sowerby@gmail.com

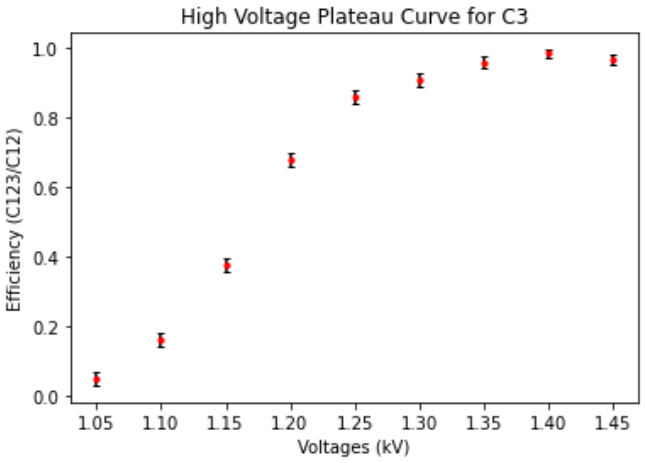

FIG. 2. Efficiency of scintillator 3 as a function of the trigger voltage. By visual inspection the base of the plateau occurs at $V_C = 1280V$.

bottom. Therefore our apparatus is fully calibrated only by calibrating the middle one.

To calibrate the middle scintillator (Discriminator 3), we define C_{123} as the number of three-fold coincidences in a given time period, and C_{12} as the number of two-fold coincidence which the particle passed through scintillators 1 and 2 in the same time period. Therefore if we set the cutoff voltage of Discriminator 3, and the record our counts for a set number of time, we will get values for C_{123} and C_{12}. Since every three-fold coincidence is also a two-fold coincidence, $C_{123} \leq C_{12}$. We want to maximize the efficiency C_{123}/C_{12}. If the equipment was calibrated perfectly, every time a muon passed through 1 and 2, it would also pass through 3 since it is in between them. In real life this is not possible, and thus our efficiency will always be strictly less than 1.

We find that if we vary the high voltage cutoff, eventually it will start reading nearly all the muons, and the efficiency will plateau. When calibrating the Discriminator, we choose a voltage at the lower-end of the plateau as to pick up all the possible muons but reduce the noise that occurs with higher voltages. This graph has been plotted in Figure 2 with counting uncertainties included.

By performing this plateauing procedure we concluded that the optimal operating high voltage for the scintillator is $V_c = 1280$ V by visual inspection of Figure 2. This high voltage was used to perform the following data analysis.

III. DATA ANALYSIS

For this experiment, we chose two time intervals and counted the number of muons for each interval. We chose $\Delta T_1 = 0.72$s in which the average number of counts was approximately 1, and fitted it with a poisson distribution. We also chose $\Delta T_2 = 31.3$s, in which the average number of counts was large, and fitted that to a gaussian distribution.

A. Poisson Fit

For the first dataset, we fitted the histrogram of counts per ΔT_1 to a poisson distribution since the probability of events occurring during our time frame was small and constant.

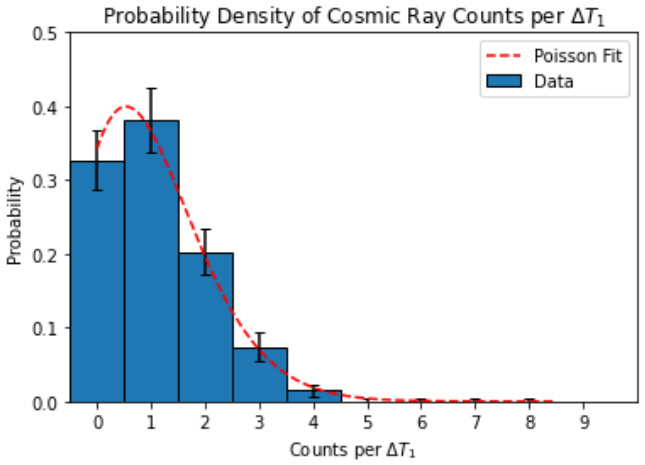

FIG. 3. Cosmic Ray counts fitted to a poisson distribution. The mean and variance of the fitted distribution $\mu = \lambda = 1.07 \pm 0.07$.

The poisson fit to the data agrees very well when comparing the mean values, but the variance of the data is smaller than the fit, even with error.

$$\mu_{\text{fit}} = \lambda_{\text{fit}} = 1.07 \pm 0.7$$
$$\mu_{\text{data}} = 1.07$$
$$\lambda_{\text{data}} = 0.96$$

The rate of cosmic rays observed in this data set can be calculated by dividing by the time interval, ΔT_1. The mean and variance in cosmic ray rate are as follows.

$$r_1 = \frac{\mu_{\text{fit}} \pm \sigma_{\text{fit}}}{\Delta T_1} = 1.48 \pm 1.43 \text{ s}^{-1}$$

B. Gaussian Fit

For the second dataset, we observed the number of counts per $\Delta T_2 = 31.3$s across several hundred trials, and plotted them in a histogram fitted with a gaussian distribution, which is more appropriate when the expected number of counts is larger, and thus more resembles a continuous distribution.

To get an appropriate looking gaussian, the data needed to be re-binned with a bin size of 2. After doing so, the fit matches the data very well. Comparing

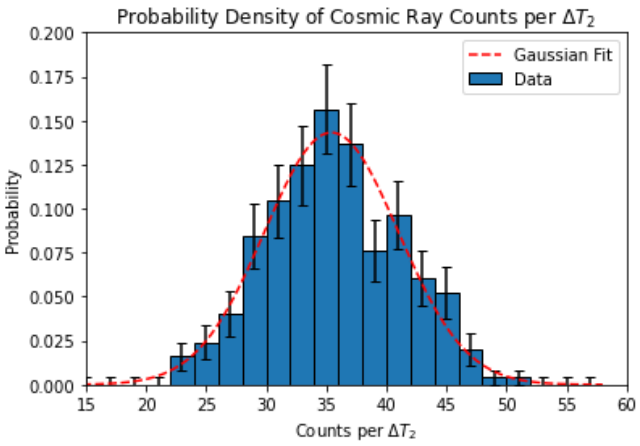

FIG. 4. Cosmic Ray counts observed within ΔT_2 fitted to a poisson distribution. The mean and standard deviation of the fit are $\mu = 35.4 \pm 0.4$ and $\sigma = 5.57 \pm 0.26$.

the parameters of the data set and the Gaussian fit, we see that

$$\mu_{\text{data}} = 35.04 \quad \mu_{\text{fit}} = 35.4 \pm 0.4$$
$$\sigma_{\text{data}} = 5.62 \quad \sigma_{\text{fit}} = 5.57 \pm 0.26$$

These values are all within errors of each other. We also notice that 66.3% of the data points lie within one standard deviation, 96.8% lie within two standard deviations, and 100% lie within three. This agrees with statistical theory for gaussian distributions very well especially given that these are discrete values.

The rate of cosmic rays for this data set can be calculated in the same way as before. The mean and variance of the cosmic ray rate are as follows.

$$r_1 = \frac{\mu_{\text{fit}} \pm \sigma_{\text{fit}}}{\Delta T_2} = 1.13 \pm 0.17 \text{ s}^{-1}$$

This value is not quite within 1 standard deviation of the data set we fitted to the poisson distribution.

Half Life Measurements*

Charlie Sowerby†
UCLA Department of Physics
(Dated: March 17, 2021)

After neutron bombarding an equal concentration of the two naturally occurring silver isotopes, they are promoted to two unstable isotopes, ^{109}Ag and ^{107}Ag in different concentrations. In this experiment we determine the optimal high voltage of a Geiger counter and calculate the detector dead time by measuring the counting rate of other radioactive isotopes. Once we have these corrections in order to measure the beta decay of the silver accurately, the decay rate silver sample is examined using the Geiger counter, fit to a sum of independent exponential decays, and the half lives are calculated.

I. INTRODUCTION

In this experiment, we measure the decay rates of two silver isotopes, ^{108}Ag and ^{110}Ag. After exposing a silver foil with approximately equal parts ^{107}Ag and ^{109}Ag to neutron bombardment, we get the two radioactive isotopes. These isotopes eventually beta decay into Cadmium emitting an electron.

$$^{n}\mathrm{Ag} \rightarrow {}^{n}\mathrm{Cd} + e^{-} \tag{1}$$

The neutron-activated sample of silver is placed inside a Geiger counter. When beta decay occurs within the silver sample, an electron is emitted into the Geiger counter, inside which the electron triggers an ionization event, in which electron-ion pairs are created. These secondary electrons then create additional ionization events in the gas-filled tube. This causes a flow of electrons to the positively biased wire, creating a current. A discriminator then records the voltage in the wire as a count if it exceeds a certain threshold. The Geiger counter is calibrated to a correct high-voltage and the dead time of the counter is taken into account.

Once the detector is calibrated, the radioactive silver isotopes is placed in the detector and the count-rate as a function of time is recorded. This decay rate is fitted to the sum of a two exponential decays to determine the half-life for each of the two samples.

II. HIGH VOLTAGE PLATEAUING OF THE GEIGER COUNTER

To perform this experiment the Geiger counter needs to be calibrated to determine the optimal tube voltage. This voltage defines the strength of the field in the tube that pulls the ionized electrons towards the central anode. When an electron enters the tube and an ionization event occurs, the speed the electrons move towards the anode depends on the operating high-voltage. If this voltage is not high enough, there won't be enough secondary ionization events generated and an avalanche won't occur. If this happens, the current in the wire won't be enough to exceed the discriminator threshold. To determine the high-voltage setting, we place a radioactive source in the tube and vary the operating voltage to see how the count rate changes as a function of the voltage. For this experiment, we have done this with two sources individually, Cobalt-60, and Sodium-22.

When our voltage is too low, the ionization event from the incoming electron will not generate an avalanche, and our counting rate will be near zero. Once we reach an appropriate cutoff, we will see a sharp increase as there is enough voltage for nearly all the initial ionization events to trigger the avalanches. We will see a plateau, and eventual increase to a continuous discharge of signal as there is enough voltage for noise to trigger a count. The plateaus for the Cobalt and Sodium sources are plotted in in Fig. 1. As a result of this analysis we have chosen our operating voltage for the Silver decay measurements to be 425 V.

III. DEAD TIME CALCULATION

The detector will have a non-negligible dead time due to reduced voltage on the wire when the ions are drifting towards the cathode during and after the ionization avalanche. When an electron enters the tube, and an avalanche occurs, and during the time it takes for all the ionization events to take place, any new electrons that enter the tube will not be observed. This is because the tube takes a small amount of time, τ, called the dead time to return to its initial state. Due to this, if there is a high counting rate, a significant amount of counts will not be observed due to this dead time, but the counting rate will be less affected if the number of counts is low, therefore we need to account for this effect. To do so we define the adjusted counting rate r' as follows.

$$r' = \frac{(\text{counts})}{(\text{time}) - \tau(\text{counts})} \tag{2}$$

Where we take the counting rate as the number of counts divided by the time in which the detector is actually observing counts. Dividing the top and bottom by time,

* Physics 180a Experiment 2
† charlie.sowerby@gmail.com

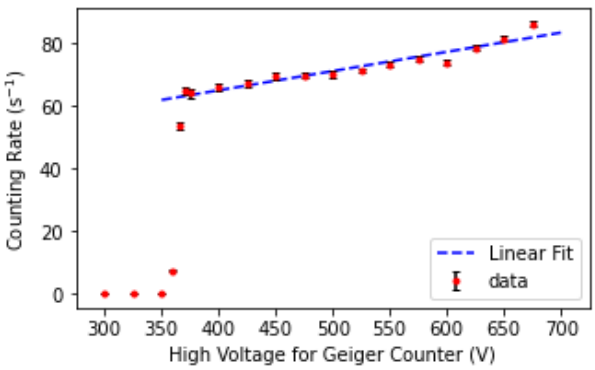

(a) Plateau for Cobalt

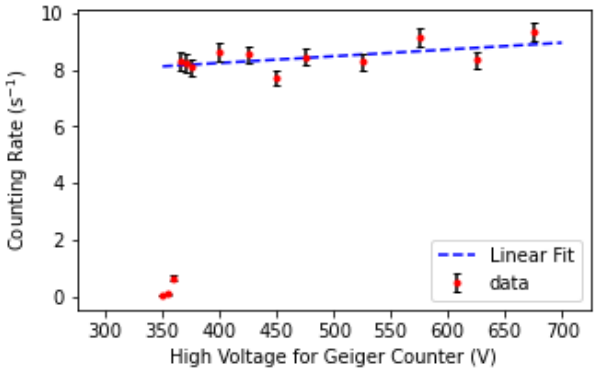

(b) Plateau for Sodium

FIG. 1: **High Voltage Plateau Calibration Plots.** Counting rate of the Geiger counter as a function of the high voltage plateau to determine optimal cutoff voltage. Experiment was performed with high-voltage of 425 V.

we can get an equation for the true counting rate r' as a function of the observed counting rate r.

$$r' = \frac{r}{1 - r\tau} \tag{3}$$

To experimentally observe the dead time, τ, we take two different radioactive elements and expose them to the detector in four different ways and observe the counting rate. First we take the two sources and observe the counting rate for each element individually, then we expose both at the same time, and finally we take data with no source. Theoretically, if r_1, r_2, r_{12} represent the true counting rate for each source and then together, then we should have the following, where d represents the counting rate with no source.

$$r_1' + r_2' = r_{12}' + d \tag{4}$$

However we don't observe this experimentally since the counting rates we observe don't account for dead time. To determine the dead time, we implemented the procedure above to find the raw counting rates. Then we used Equation (2) to get the following, analytically determining the dead time.

$$\frac{r_1}{1 - r_1\tau} + \frac{r_2}{1 - r_2\tau} = \frac{r_{12}}{1 - r_{12}\tau} + d \tag{5}$$

Where we can solve a cubic polynomial analytically for τ. To obtain the counting rate for each sample, we let the detector run for a fixed amount of time for each sample, and then took the total number of counts divided by the total time. In doing this procedure we obtain the values in Table 1.

Solving the cubic polynomial yields three values for dead-time, we selected the one closest to the reported value in the lab manual. The uncertainty in this calculation was neglected as propagating it through the analytical solution would have taken too long.

$$\tau = 0.000356$$

All of the counting rates for silver were adjusted using the above dead time.

IV. DATA ANALYSIS

To calculate the half life of the two silver isotopes, four trials were performed exposing the silver source to the Geiger counter for approximately 500 seconds each trial. The number of counts was recorded every 50 milliseconds, and the count rate for each of these time-steps was adjusted according to the dead time correction. The count rate was then plotted as a function of time. The data was fitted to a sum of two exponential decays, one for each of the two silver isotopes.

$$r = Ae^{-\lambda_1 t} + Be^{-\lambda_2 t} \tag{6}$$

After fitting the count rate to the sum of the two decays, we can isolate the decay constants λ_1, λ_2. The half life of each of the two silver decays is the amount of time it takes for half the sample to decay. In other words, the count rate will be half of its original value since it is proportional to the amount of sample left .

$$\frac{A}{2} = Ae^{-\lambda T_{1/2}} \longrightarrow T_{1/2} = \frac{\log(2)}{\lambda} \tag{7}$$

After fitting the curve to two exponential decays, we determine the values of λ_1, λ_2 with associated errors. The

TABLE I: Counting Rates for Dead Time Calculation

Sample	Counting Rate (counts/sec)
Cobalt	266.5 ± 1.2
Cesium	112.81 ± 0.79
Both	359.0 ± 1.41
Background	0.385 ± 0.046

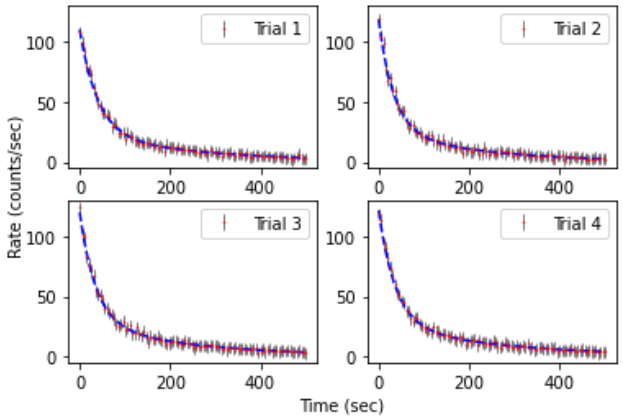

(a) Decay for Individual Trials

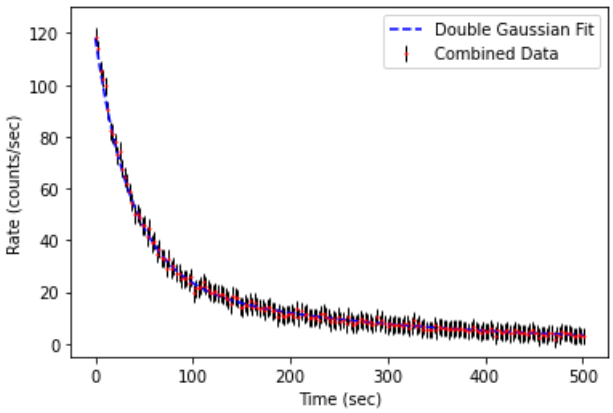

(b) Combined Data

FIG. 2: **Exponential Decay of ^{108}Ag and ^{110}Ag.** Calculated Half-lives for the combined data set are $T_{110} = 25.5 \pm 2.7$ and $T_{108} = 175. \pm 33.$ seconds. See Table 2 for Half-lives for each trial.

error on the half-life is given by the following formula.

$$\delta T_{1/2} = \frac{\log(2)\delta\lambda}{\lambda^2} \tag{8}$$

TABLE II: Half-life values for each trial.

Trial	^{110}Ag Half-life (s)	^{108}Ag Half-life (s)
1	27.7 ± 3.1	$179. \pm 39.$
2	22.8 ± 2.6	$145. \pm 26$
3	24.1 ± 2.7	$160. \pm 27.$
4	25.2 ± 2.6	$174 \pm 31.$
Combined	25.4 ± 2.0	$163. \pm 21.$

After running all four trials, a final combined plot of data is obtained by performing an error-weighted average of the data at each time t. The uncertainty in the count rate at each time t would be calculated by the formula

$$\frac{1}{\sigma^2} = \sum_{i=1}^{4} \frac{1}{\sigma_i^2} \tag{9}$$

The combined data appears in Fig 2b. The calculated half-life values for each trial as well as the value for the combined data set appear in Table 2. The final values appear to be within uncertainty of the measured values of $T_{1/2} = 142.2 \pm 6$ for ^{108}Ag and $T_{1/2} = 2.46 \pm 0.01$ for ^{110}Ag.

Beta Spectrometer*

Charlie Sowerby†
UCLA Department of Physics
(Dated: March 17, 2021)

To measure the beta spectrum of unstable Cesium-137, we place a sample in a solenoidal spectrometer attached to a Geiger counter. The spectrometer selects electrons by momentum, and we observe the rate of measured decay electrons as a function of their momentum. The observed spectrum is corrected as the range of allowed momenta is linearly proportional to the momentum. The true spectrum is fitted to two Gaussian distributions to determine the internal conversion coefficients of the electrons. Subtracting these conversion electrons, we linearize the spectrum to find the beta endpoint energy and it is used to calculate the comparable half life.

I. INTRODUCTION

In this experiment we observe the beta decay spectrum of Cesium-137 through the use of a solenoidal spectrometer and a Geiger counter. The spectrometer uses a constant magnetic field to select electrons with a given momentum, and the Geiger counter counts the electrons as a function of the allowed momenta. The spectrum includes the electrons produced through beta decay from Cesium-137 to an excited state of Barium-137, and it also contains two peaks from ejected electrons from internal conversion as the excited Barium decays into its ground state. From this spectrum, the conversion coefficients are measured, the beta endpoint energy is observed, and the log(ft) value is calculated.

The decay we are measuring is the beta decay of Cesium-137, which is represented by this equation.

$$^{137}\mathrm{Cs} \rightarrow {}^{137}\mathrm{Ba} + e^- + \bar{\nu_e}$$

During this decay, 5.4% of the time the resulting Barium is in the ground state, but in the other 94.6% of the time the result is an excited state, which has energy approximately 662 keV more than the ground state. This excited state de-excites into the ground state by means of photon emission or internal conversion, where an electron is ejected with the excited state energy minus the binding energy of the electron. We can observe separate peaks of the beta spectrum as well as ejections of the K and L shell electrons.

II. EXPERIMENTAL DESIGN

To perform this experiment, Cesium-137 source was positioned along the axis of a solenoid, through which a current was driven to produce a magnetic field along the parallel axis towards the detector. The solenoid is contained in a vacuum tube to prevent any air molecules from altering the results. Due to the uniform magnetic field, electrons moving along the tube would spiral in a helical shape with a constant parallel velocity.

The magnetic field in the solenoid can be approximated by the formula $B = \mu_0 n I$ where n is the number density of the coils and I is the current in the wire. The current is measured by applying a voltage across a resistive element, whose resistance is known very precisely. This shunt voltage is varied across multiple trials.

Near the Cesium source, inside the solenoid, inner and outer angle selecting baffles were placed such that all but a narrow annulus would absorb emitted electrons. These angle selecting baffles only allowed particles emitted with an angle between 12° and 16° to pass through. The lead inner baffle also contained helicoidal baffles such that particles could only move with helical paths in the counterclockwise direction. This eliminated all particles moving with positive charges. These angle selecting baffles ensured that only particles with helical paths that have the correct trajectory into the detector. Since the wavelength of the oscillation is linearly proportional to the strength of the magnetic field, and that magnetic field is proportional to the shunt voltage, we can determine a counting rate across the Geiger Counter as a function of the shunt voltage.

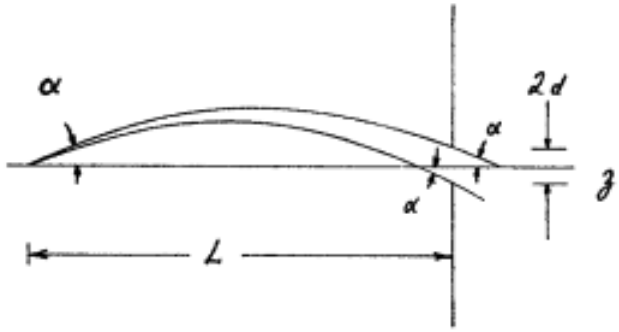

FIG. 1. Diagram of how angle selecting baffles only allow particles oscillating with a wavelength of $2L$ into the detector.

When taking data for this experiment, the shunt voltage was not able to be maintained at a constant value, so the shunt voltage fluctuated during the trial. As a re-

* Physics 180a Experiment 3
† charlie.sowerby@gmail.com

sult the allowed momenta values have uncertainties. For the purposes of this experiment, the uncertainty in the momentum value due to the range of allowed momenta was ignored.

A. Calibration of Equipment

In this experiment, we assume the Geiger counter was already calibrated, as the technique was performed in the previous experiment. For the solenoid, the constant of proportionality between the shunt voltage and the momenta that are selected is known. Therefore we can write the counting rate as a function of the selected momentum. Since the baffles allow a range of angles through, as the magnetic field gets larger, the shallower the oscillations become, and the larger the number of electrons are allowed into the detector. This number is linearly proportional to the momentum of the selected particles. Therefore to correct our data, we need to divide the counting rate by the momentum of the selected particles.

III. DATA ANALYSIS

After obtaining a corrected plot of the rate of electron emission as a function of its momentum, we can do one final adjustment, by comparing the internal conversion peaks with known binding energies. Therefore in this experiment the observed momenta were adjusted by a small factor (~ 1.03) such that the K shell peak matched with the experimental value. This raw data is plotted in Figure 2.

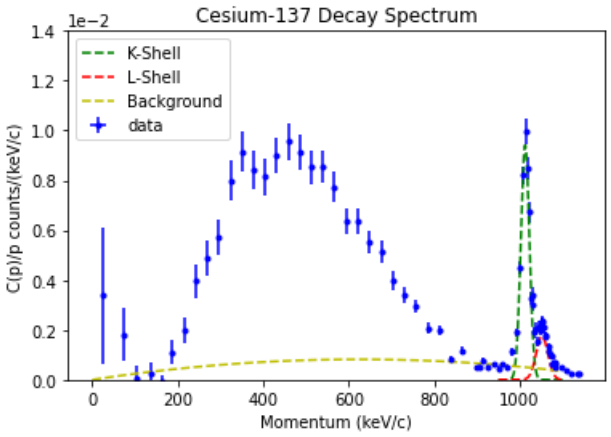

FIG. 2. Electron observation rate as a function of momentum from the Cesium sample. The internal conversion peaks are fitted to a gaussian distributions with peaks at 1012.5 ± 0.7 and the background fitted to a second order polynomial.

The background noise in Figure 2, is most likely due to the 5.4% chance of decaying directly to the ground state, in which case we would observe a larger energy much lower amplitude beta spectrum. In this case it was fit to a second order polynomial with a zero constant term as the underlying beta would go to zero at zero momentum.

A. Conversion Coefficients

When the daughter nucleus is in its excited state, we want to determine the relative probability of the means of de-excitation. To do so, we recognize that every time we observe a beta decay in the plotted beta spectrum, that it needs to de-excite somehow. Therefore the total number of electrons observed in the beta spectrum will equal the total number of electrons observed in internal conversion peaks plus the number of photons emitted. We cannot measure the number of photons emitted, but since there is only one unknown, we can solve for that number. The conversion coefficient for each electron shell is the probability of an electron from that shell being ejected divided by the probability of a photon being emitted.

$$\alpha_K = \frac{N_K}{N_\gamma} = \frac{N_K}{N_\beta - (N_K + N_L)}$$
$$= \frac{0.23(2)}{3.37(7) - (0.059(8) + 0.23(2))} = 0.0758(63)$$
$$\alpha_L = \frac{N_L}{N_\gamma} = \frac{N_L}{N_\beta - (N_K + N_L)}$$
$$= \frac{0.059(8)}{3.37(7) - (0.059(8) + 0.23(2))} = 0.0193(25)$$

From the data the M shell peak was unable to be identified, so it was unable to be included in the calculation for the conversion coefficients. The value of α_L is almost exactly equivalent to the known value of the conversion coefficient for the L and M shells added together. Our value for the K shell is too low. This could be due to the inability to get through the background interference.

The errors for N_K and N_L were calculated given the uncertainty on the gaussian fits for the internal conversion electrons. For the beta spectrum, the error was analytically for each term in the numerical integration.

B. Beta Endpoint Energy

This endpoint energy represents the maximum possible kinetic energy of the ejected electron. This represents a scenario in which the ejected neutrino has zero kinetic energy, and allows us to measure the rest mass of the neutrino.

According to theory, we can model the shape of the beta distribution

$$N(p) \propto p^2 \left(Q - T_\mathrm{e}\right)^2 F\left(Z', p\right) \left|M_{fi}\right|^2 S(p, q)$$

Where Q is defined by the difference in the initial and final nuclear mass energies from the decay, i.e. the decay energy. T_e represents the kinetic energy of the beta

electron. The factor $p^2(Q-T_e)$ is derived from the number of final states accessible to the neutrino and electron. $F(Z',p)$ represents the Fermi function, which is used to account for the coulomb effects of the daughter nucleus. Finally the terms $|M_{fi}|^2 S(p,q)$ which is the nuclear matrix element, with correction for electron and neutrino momentum dependence from forbidden terms.

If we are in a case with no forbidden decays, we can approximate this function to

$$N(p) \propto p^2 \left(Q - T_\mathrm{e}\right)^2 F\left(Z', p\right)$$

In which case we get $(Q-T_e) \propto \sqrt{\frac{N(p)}{p^2F(Z,p)}}$. Therefore if we plot the right hand side as a function of kinetic energy of the electron, we get a linear plot, called a Kurie Plot. Observing where the line crosses the x-axis gives us the Q value for this decay.

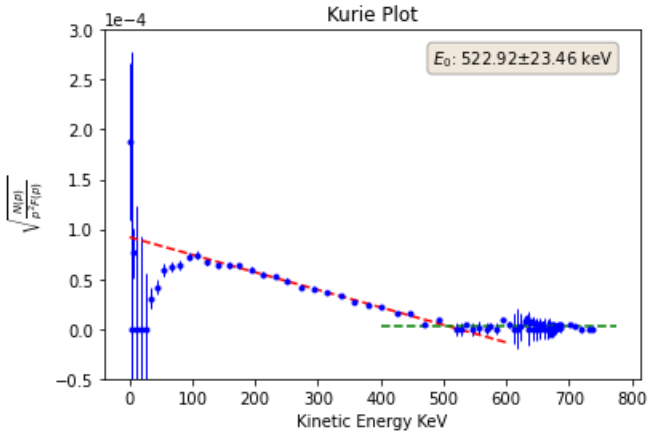

FIG. 3. Linearized Beta spectrum to determine the endpoint energy. The green line is the line $y=0$. The red line is a linear fit to the beta spectrum of the form $y=ax+b$ with parameters $a=(-1.76\pm0.06)\times10^{-7}$ and $b=(9.19\pm0.24)\times10^{-5}$.

The measured endpoint energy is as follows.

$$E_0 = 522. \pm 23.\ \mathrm{keV}$$

In this calculation, the error was propagated through the quantity $\sqrt{\frac{N(p)}{p^2F(Z,p)}}$, where the Fermi function was treated as an exact value, as propagating the uncertainty in momentum through a Gamma functions is not possible analytically. The error formula was derived as follows, where $K = \sqrt{\frac{N}{p^2F(p)}}$

$$\begin{aligned}\delta K &= \sqrt{\left(\frac{\partial K}{\partial N}\delta N\right)^2 + \left(\frac{\partial K}{\partial p}\delta p\right)^2} \\ &= \sqrt{\frac{(\delta N)^2}{Np^2} + \frac{4N(\delta p)^2}{p^4}}\end{aligned} \tag{1}$$

C. Comparable Half Life

To determine the decay rate of this beta decay, if we use the Fermi golden rule for transition rates, and if we use the allowed approximation to expand the electron and neutrino free particle wavefunctions and keep only the first term, a constant 1, we get the following equation for the differential decay rate.

$$d\lambda = \frac{2\pi}{\hbar} g^2 \left|M_{\mathrm{fi}}\right|^2 (4\pi)^2 \frac{p^2 dp q^2}{h^6} \frac{dq}{dE_f} \tag{2}$$

Where the constant g represents the strength of the interation, q represents the neutrino momentum. The value of q represents the neutrino momentum, where we can write $qc = Q - T_e$ since the neutrino has no mass according to the Fermi theory. We know the final energy of the decay is $E_e + E_\nu = E_e + qc$, therefore the differential $\frac{dq}{dE_f} = \frac{1}{c}$ at a given electron energy.

Integrating over all the allowed electron momenta, we get

$$\lambda = \frac{g^2 \left|M_{\mathrm{fi}}\right|^2}{2\pi^3\hbar^7c^3} \int_0^{p_{\max}} F\left(Z', p\right) p^2 \left(Q - T_e\right)^2 dp \tag{3}$$

Since the integral only depends on the endpoint energy and the atomic number of the daughter nucleus, we can write this integral as the following, normalized so it is dimensionless.

$$f\left(Z', E_0\right) = \frac{1}{\left(m_\mathrm{e}c\right)^3 \left(m_\mathrm{e}c^2\right)^2} \int_0^{p_{\max}} F\left(Z', p\right) p^2 \left(E_0 - E_\mathrm{e}\right)^2 dp \tag{4}$$

But since we know the decay rate of $Cs-137$, we know that the half life is 30.17 years, and that $\lambda = \ln(2)/t_{1/2}$. Therefore we see the matrix element $|M_{fi}|^2$ is proportional to the $ft_{1/2}$ value. This matrix element

$$ft_{1/2} = 0.693 \frac{2\pi^3\hbar^7}{g^2 m_\mathrm{e}^5 c^4 \left|M_{\mathrm{fi}}\right|^2} \tag{5}$$

Therefore by numerically performing this integral, we can get an estimate on the matrix element $|M_{fi}|^2$ which tells us whether we are measuring a probable transition. Since the value of $ft_{1/2}$ will usually be extremely large, we report the value of $\log_{10}(ft_{1/2})$

For this experiment, with the beta endpoint energy of 514.44 keV, and the Z value of Barium 56, we can perform the numeric integration, and multiply it with the half life of Cs-137 to get

$$\log(ft_{1/2}) = 9.587$$

This value could correspond to a transition that is either allowed, first forbidden unique, or first forbidden non-unique.

To calculate the uncertainty on the log(ft) value, the value of E_0 would have been varied around its equilibrium

value in a gaussian distribution with a standard deviation with the reported error above. The value of log(ft) would have been calculated for each value and then fitted to a gaussian distribution, but for the purposes of this report that calculation was not attempted.

The Compton Effect*

Charlie Sowerby†
UCLA Department of Physics
(Dated: March 17, 2021)

To measure the Compton scattering of the two gamma decay modes of Cobalt-60, three proportional detectors were placed around the scattering center to observe the scattered photon while a fourth detector was placed at the scattering center to observe the recoil electron. After calibrating the detectors, three measured photon energy as a function of the scattering angle. A 2D histogram of these energies allowed us to distinguish the two decay modes, and the scattered photon energy as a function of the scattering angle was matched to theoretical predictions for each initial energy.

I. INTRODUCTION

In this experiment, we measure Compton scattering of gamma decay photons from Cobalt-60. The Cobalt decays in two different gamma modes, emitting photons with energy 1.173 and 1.333 MeV towards a scattering center. These photons are collimated into a straight line. Three plastic scintillators are positioned around the scattering point at measured angles with respect to the scattering angle. These crystals are connected to PMT's that are operated with a positive voltage to produce a voltage proportional to the deposited energy. This voltage is then passed to an Analog-to-Digital Converter(ADC) with a resolution of 4096 values. These values can be calibrated using known-energy photons and are proportional to the energy. Three detectors, named Abel, Baker, and Cain are positioned around the scattering center at known angles, and a fourth, fixed detector, is placed at the scattering sample to observe the energy of the recoil electron that the photon has scattered off. Each of these detectors is calibrated individually.

After the detectors are calibrated we observe scattered photons from a cobalt source over several trials in which the detectors are positioned at various angles. The data points observed from the photons scattered with each of the two initial energies are separated, and the scattered energy is plotted as a function of the scattering angle.

In this paper we verify the Compton Scattering formula for the wavelength of the scattered photons.

$$\lambda - \lambda_0 = \frac{h}{m_e c}(1 - \cos\theta) \tag{1}$$

II. CALIBRATION OF EQUIPMENT

To calibrate the detectors, samples of Cobalt-60, Sodium-22, Cesium-137, and Barium-133 are placed near the detectors, and they are allowed to accumulate data, outputting an ADC value every time a photon is observed. For each of the samples and detectors, the ADC values are histogrammed, producing 24 plots similar to Figure 1. Two other histograms of ADC values for observed photons can be found in Appendix A. Those plots feature Cobalt as measured by the Abel detector and Barium as measured by the Baker detector.

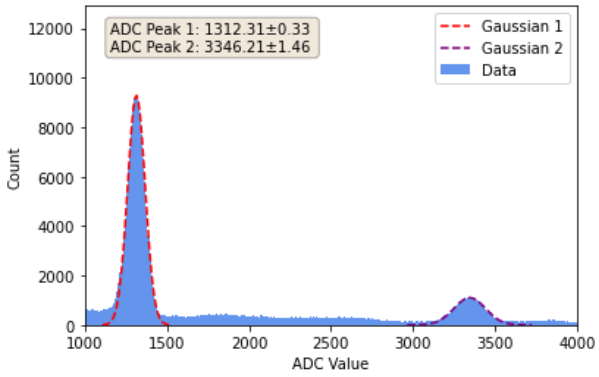

FIG. 1: Histogram of photon energies from ^{22}Na decay as measured by the Cain detector. Peaks correspond to known energy values for gamma decay of ^{22}Na with energies 511 and 1274 keV.

In each figure clear peaks of gaussian distributions are observed around the ADC value representing the gamma

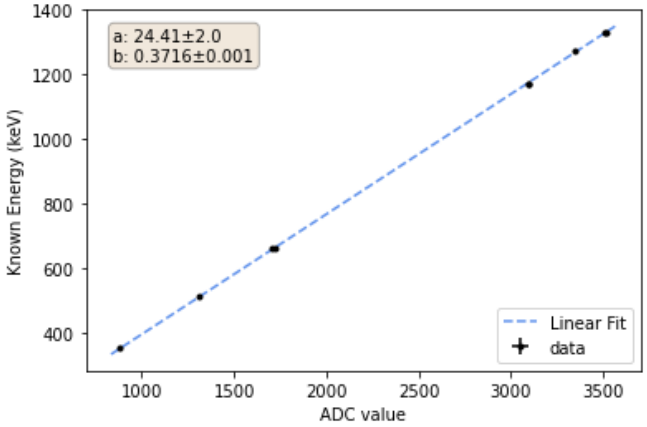

FIG. 2: Linear relationship between ADC value and energy for the Cain detector.

* Physics 180a Experiment 4
† charlie.sowerby@gmail.com

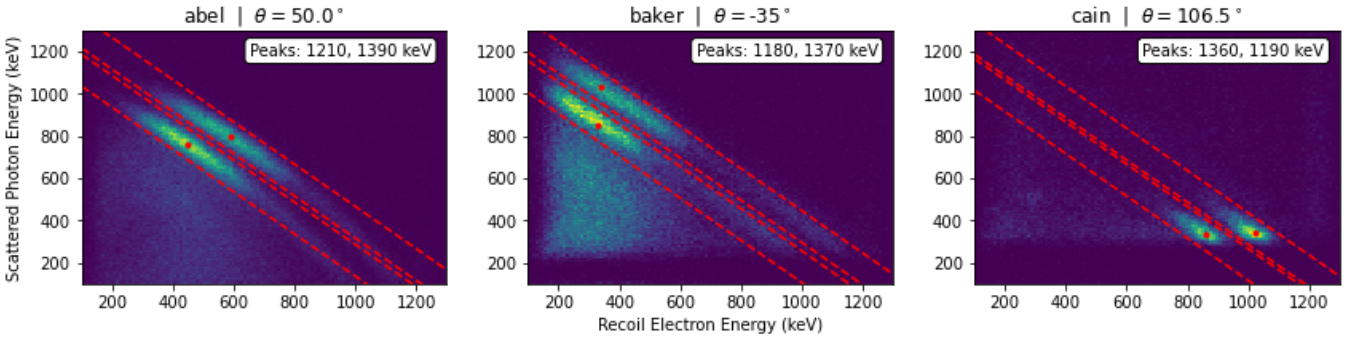

FIG. 3: **2D Decomposition of Photon and Electron Energy.** Plotted energy coincidence between detectors sliced along rows of constant total energy around the two maximum values for one trial. The total energy for each peak appears on the figure.

decay energy of each sample. These known energy values are plotted against the mean of the gaussian distributions for each sample. As this procedure is repeated, it is obvious that a linear relationship forms between ADC value and energy, and for each detector a calibration plot is fitted to a line. For each of the four detectors we have a calibration plot that maps ADC values to energies linearly. Figure 2 shows the calibration plot for the Cain detector, the other three can be found in Appendix A.

III. DATA ANALYSIS

To take actual data, only the Cobalt-60 source is used, but seven trials are performed each with the Abel, Baker, and Cain detectors positioned at a different scattering angle for each trial. Since we only want to take data when a Compton scattering event occurs, we require a coincidence between any one of the three photon detectors and the fixed detector, that way we only take data when we observe a scattered photon at the same time as a recoil electron. The ADC values from the detectors are then converted into energies, and we get a number of counts as a function of energy for each detector.

If there were only one energy photon being scattered, this would be all we would need to determine the Compton scattering energy formula, as we would observe a gaussian with a single peak for each detector whose angle with respect to the scattering angle we would know. Unfortunately, since Cobalt has two gamma decays with different energies, we need to separate the peaks as they appear on top of each other. In Figure 3 we have plotted 2D histograms in energy of the photon detectors (Abel, Baker, Cain) on the y-axis, and the electron fixed detector on the x-axis. Due to energy conservation, the sum of the energies for the scattered photon and recoil electron will equal the initial photon energy, therefore lines with slope -1 represent surfaces of constant total energy. In Figure 3 we can discern two individual peaks with separate total energy for each detector.

In Figure 3, the two brightest peaks are highlighted

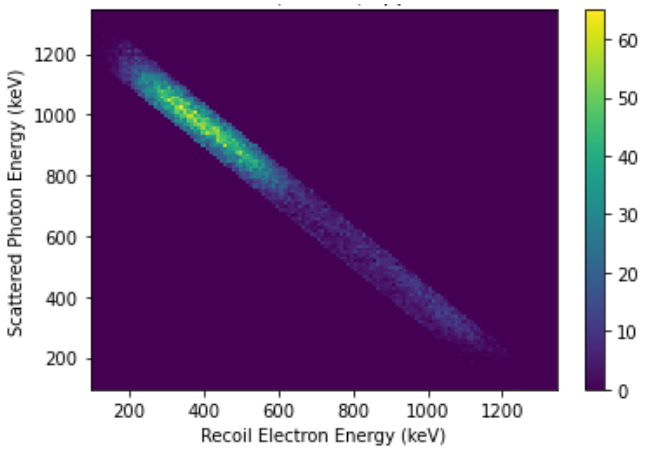

FIG. 4: Isolated higher-energy peak from the Baker detector in Figure 3.

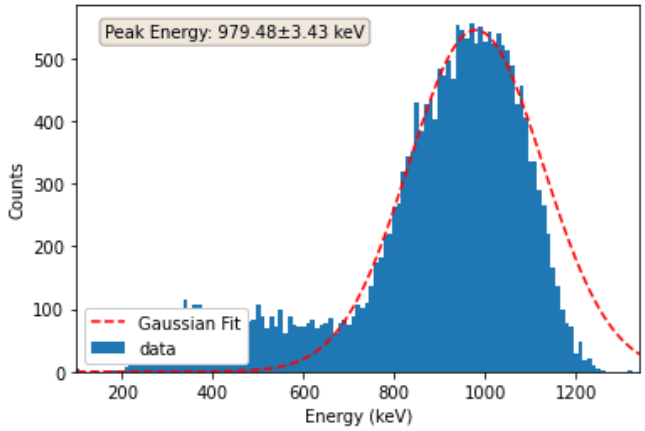

FIG. 5: Data from Figure 4 projected onto the y-axis.

and cuts of total energy ±75 keV are taken above and below the peak value. These are shown in red in Figure 3. These cuts are then isolated into their own figures. The data shown in Figure 4 represents the higher energy slice

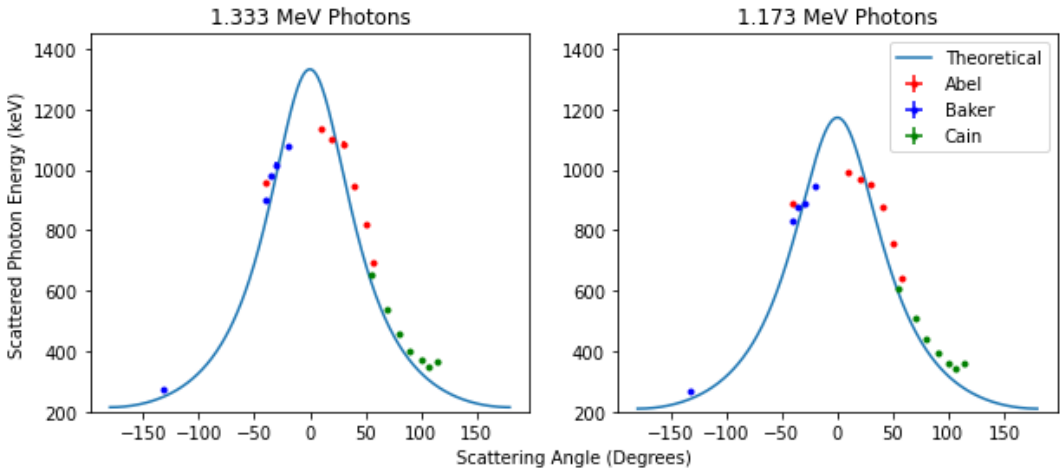

FIG. 6: **Observed Energies of Compton Scattered Photons.** Observed energies of scattered gamma rays with initial energies of 1.333 and 1.173 MeV as a function of the scattering angle.

from the baker detector shown above in Figure 3. The 2D histogram values are then summed along horizontal cuts, recovering the single gaussian peak from the baker detector, positioned at $\theta = 35°$. This data, shown in Figure 5, was then fitted to a gaussian, and the mean was determined. Therefore we get a measurement for the energy value of photons scattered at 35° with a single initial energy scattered. This procedure was repeated across all detectors and all trials for both the higher and lower energy peak, and the data is plotted in Figure 6.

When converting from ADC to an energy value, errors in the calibration were regarded as negligible as they are so small. Counting errors were used for each bin in the 2D histogram in Figure 2. This error was carried through the isolation procedure to Figure 4, and then summed using equation 2 below to obtain an error value on each of the bins in the 1D projected histogram in Figure 5, for each of the trials and detectors.

$$\delta x_j = \sqrt{\sum_i (\delta x_{ij})^2} \tag{2}$$

Where δx_{ij} represents the uncertainty on the point in the 2D histogram with photon energy j and electron recoil energy i. It is summed across all electron recoil energies, albiet the uncertainty in the region outside the cut is set to zero.

IV. RESULTS

In Figure 6, we see all the peak energies plotted as a function of the scattering angle. The predicted value curve comes from Equation (1), and is calculated using the known values of Cobalt-60 gamma decay: 1.173 and 1.333 MeV.

$$E_s = \frac{E_0}{1 + \frac{E_0}{m_e c^2}(1 - \cos\theta)} \tag{3}$$

In Figure 4, the uncertainty in the scattering angle was given as ±1° for every detector, as positioning the detectors at exact angles is difficult due to their size. The uncertainty in the scattered photon energy represents the uncertainty of the mean of the gaussian distribution pictured in the upper left hand corner of Figure (5). In general, these distributions were nicely shaped to Gaussians, so this uncertainty ended up being rather low, despite deviation from the theoretical predicted value. The uncertainty values in both x and y in Figure 6 are smaller than the data points. The data in Figure 6 are color coded for each detector as the calibration for certain detectors was not perfect, most notably Abel, and we how the data points deviate from the theoretical value given which detector was used. In general the data very nicely follows the theoretical prediction for Compton scattering.

Appendix A: Calibration Figures

As there were four detectors to calibrate, and measurements were taken from 6 different samples, there were 24 plots generated Similar to Figure 1. Figure 7 contains two examples from that set of calibration plots.

These 24 histograms translated to a linear calibration plot for each of the four detectors used pictured in Figure 8.

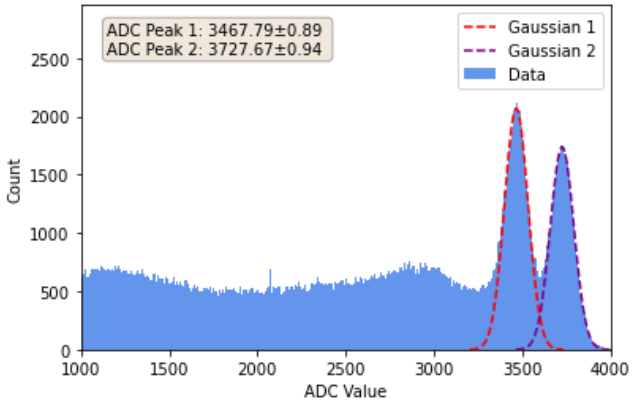

(a) Abel: Cobalt

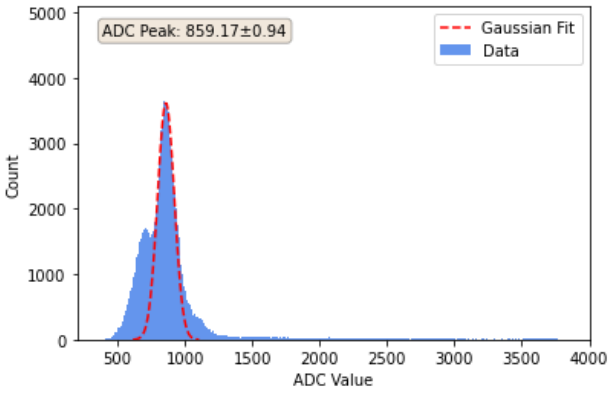

(b) Baker: Barium

FIG. 7: Histogram of photon energies from ^{60}Co and ^{133}Ba as observed by the Abel and Baker detectors. The peaks in (a) correspond to known energies of 1173 and 1332 keV, and the peaks in (b) correspond to a known energy 365 keV.

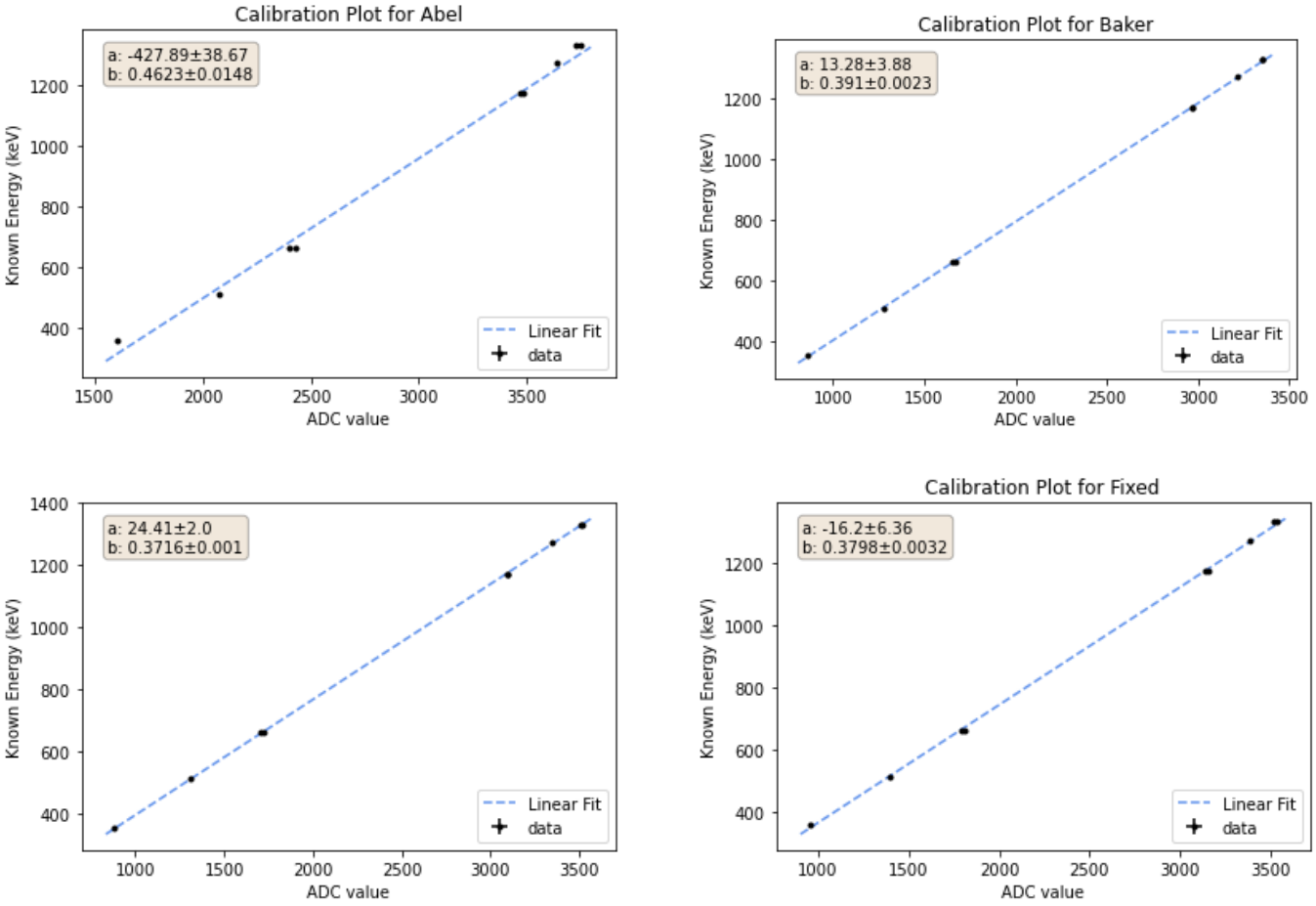

FIG. 8: Linear ADC to energy calibration for each detector used to measure Compton scattering.